

## Inelastic pion scattering from ${}^3\text{H}$ and ${}^3\text{He}$

B. L. Berman, G. C. Anderson,\* W. J. Briscoe, A. Mokhtari,<sup>†</sup> and A. M. Petrov<sup>‡</sup>

*Center for Nuclear Studies, Department of Physics, The George Washington University, Washington, D.C. 20052*

M. E. Sadler

*Department of Physics, Abilene Christian University, Abilene, Texas 79699*

D. B. Barlow,<sup>§</sup> B. M. K. Nefkens, and C. Pillai<sup>§</sup>

*Department of Physics, University of California at Los Angeles, Los Angeles, California 90024*

(Received 23 November 1994)

Cross sections have been measured for the inelastic scattering of  $\pi^+$  and  $\pi^-$  mesons from  ${}^3\text{H}$  and  ${}^3\text{He}$  in the 10-MeV interval just above the breakup thresholds, for incident pion energies of 142, 180, and 220 MeV and scattering angles of  $40^\circ$ ,  $60^\circ$ ,  $80^\circ$ ,  $90^\circ$ , and  $110^\circ$ . No significant departure from unity is observed for the ratios of charge-symmetric cross sections. Comparisons are made with elastic pion-scattering and inelastic electron-scattering data.

PACS number(s): 21.45.+v, 24.80.Dc, 25.10.+s, 25.80.Ek

### I. INTRODUCTION

Pion scattering provides a means of exploring the structure of nuclei in a way which depends on the distributions of protons and neutrons within the nucleus. As reported in earlier papers [1–4], elastic pion scattering from the mirror nuclei  ${}^3\text{H}$  and  ${}^3\text{He}$  has revealed a violation of nuclear charge symmetry. This effect is significantly larger than can be accounted for by the Coulomb interaction, and has been attributed to the differences in the proton and neutron radii for these nuclei. A prominent feature of the  $\pi^-$ - ${}^3\text{H}$  and  $\pi^+$ - ${}^3\text{He}$  elastic-scattering angular distributions is the non-spin-flip dip near  $75^\circ$  in the center-of-mass system. This is a consequence of the Pauli principle, which inhibits spin-flip elastic scattering from the neutron pair in  ${}^3\text{H}$  and the proton pair in  ${}^3\text{He}$ , in conjunction with the strong angular dependence of  $\pi$ -N elastic scattering. The two ratios of the charge-symmetric cross sections, which we call the simple ratios, are

$$r_1 = d\sigma(\pi^+ - {}^3\text{H})/d\sigma(\pi^- - {}^3\text{He})$$

and

$$r_2 = d\sigma(\pi^- - {}^3\text{H})/d\sigma(\pi^+ - {}^3\text{He}).$$

The ratios  $r_1$  and  $r_2$  are dominated by scattering from the unlike (odd, unpaired) and like (even, paired) nucleons, respectively, of the trinucleon system in the angular region of the non-spin-flip dip, that extends approximately from  $50^\circ$  to  $90^\circ$ . The superratio  $R$ , originally defined in Ref. [1], is the product of  $r_1$  and  $r_2$ .

Pauli blocking does not apply to inelastic pion scattering, in which the trinucleon breaks up. There is no reason to expect these reaction channels to demonstrate a large violation of charge symmetry. The charge-symmetric ratios are expected to be close to unity, since the cross sections are determined primarily by the charge-symmetric elementary pion-nucleon amplitudes, modified by the effects of the nuclear medium.

The data on inelastic pion scattering presented here were obtained simultaneously with those of Ref. [4]; they did not require extra beam time. The results are subject to larger systematic uncertainties than the elastic-scattering data, because the inelastic data are distributed over all missing energies above the breakup thresholds, while the elastic-scattering events are concentrated in a single peak. The inelastic data therefore require much larger background subtractions than do the elastic data. Also, the ratio technique, which has proven to be so effective for elastic scattering, cannot be applied directly because the breakup thresholds for  ${}^3\text{H}$  and  ${}^3\text{He}$  differ by 0.8 MeV. Therefore, the cross sections were obtained for the first 10-MeV interval above the breakup thresholds.

### II. EXPERIMENT AND DATA REDUCTION

The experimental setup and procedures, as well as details of the beam monitoring, were identical to those of Ref. [4]; we shall summarize them only briefly here.

The measurements were carried out at the Energetic Pion Channel and Spectrometer (EPICS) at the Los Alamos Meson Physics Facility (LAMPF). The hydro-

\*Present address: Science Magazine, Washington, DC 20005.

<sup>†</sup>Present address: Mashhad University, Mashhad, Iran.

<sup>‡</sup>Present address: Centre d'Etudes Nucleaires de Saclay, 91191 Gif-sur-Yvette, France.

<sup>§</sup>Present address: Los Alamos National Laboratory, Los Alamos, NM 87545.

gen and helium samples were contained in high-pressure gas cells, 2.5 l in volume, at 30 atm pressure; the sample masses were 18 g for  $^3\text{H}$  and 9 g for  $^3\text{He}$ . The radioactivity of the  $^3\text{H}$  samples was 186 kCi. The sample masses were determined with an accuracy of 0.3% by direct weighing before and after the experiment, and verified by PVT measurements. The target cells were stacked in a ladder-type sample changer, together with  $^2\text{H}$  and  $^1\text{H}$  cells and an empty target cell for normalization and background measurements. The cells were irradiated in sequence (see Ref. [4] for details).

Data were obtained at laboratory pion kinetic energies  $T_\pi = 142, 180,$  and  $220$  MeV at laboratory scat-

tering angles  $\theta_L = 40^\circ, 60^\circ, 80^\circ, 90^\circ,$  and  $110^\circ$  for 142 MeV;  $40^\circ, 60^\circ, 80^\circ,$  and  $110^\circ$  for 180 MeV; and  $40^\circ, 60^\circ,$  and  $80^\circ$  for 220 MeV. Background spectra obtained with the empty target were normalized using the measured relative beam flux and were then subtracted from the other spectra as appropriate. Examples of both raw and background-subtracted spectra are shown in Fig. 1. One can readily observe that the background rates for these typical data range from about 30 to 70% for inelastic scattering, while they are only a few percent for elastic scattering. Absolute yields were determined from comparisons with  $\pi$ - $d$  and  $\pi$ - $p$  elastic scattering (see Ref. [4]). The relative detector acceptance as a function of position

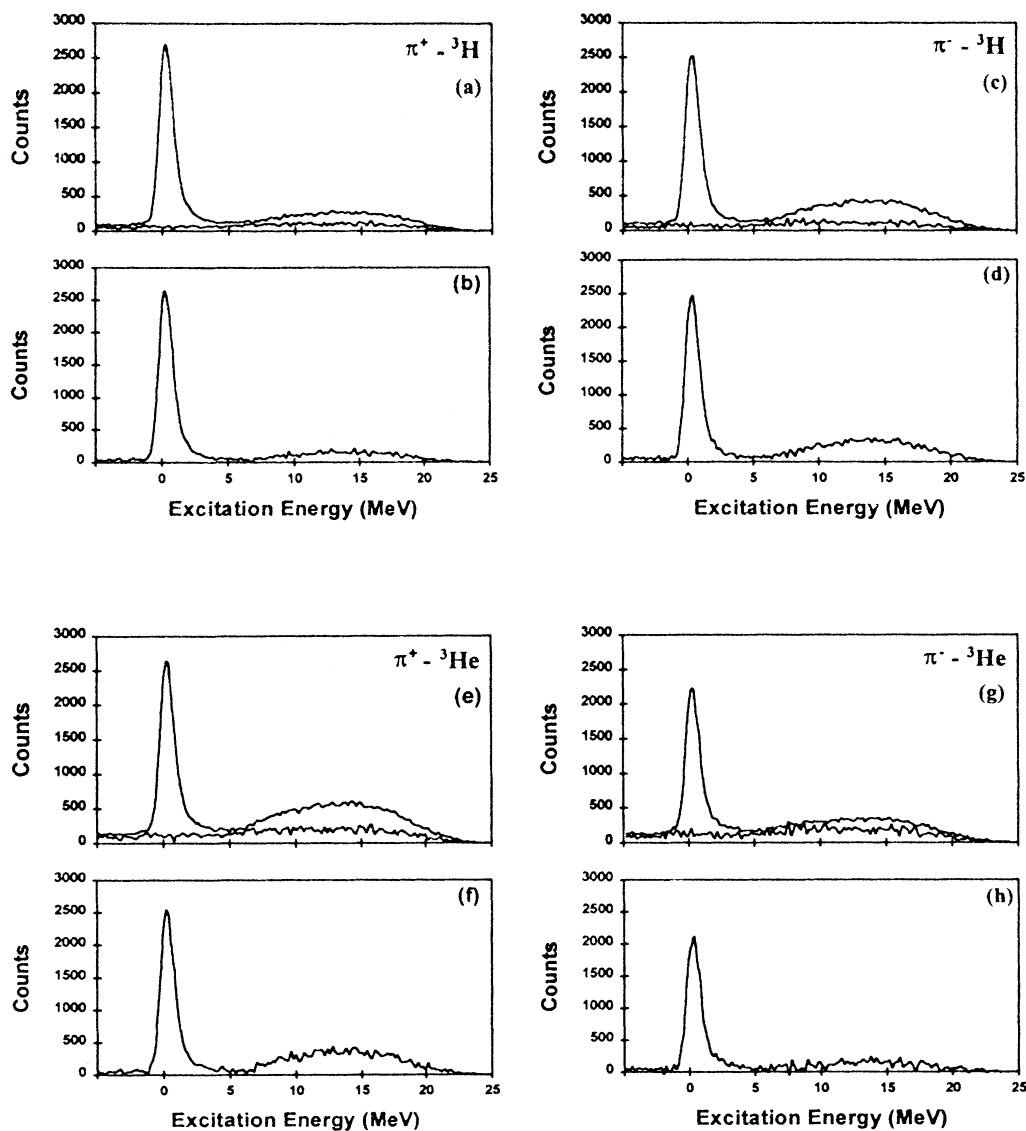


FIG. 1. Raw and background-subtracted spectra for  $\pi^+$  and  $\pi^-$  scattered from  $^3\text{H}$  and  $^3\text{He}$  at 142 MeV and  $60^\circ$ : (a)  $\pi^+$ - $^3\text{H}$  scattering; top curve, sample-in data, bottom curve, normalized (for equal pion-beam flux) sample-out data; (b)  $\pi^+$ - $^3\text{H}$  scattering, (sample-out) background-subtracted data; (c) and (d) the same as (a) and (b) for  $\pi^-$ - $^3\text{H}$  scattering; (e) and (f) the same for  $\pi^+$ - $^3\text{He}$  scattering; (g) and (h) the same for  $\pi^-$ - $^3\text{He}$  scattering. No corrections for acceptance (see Fig. 2) have been applied.

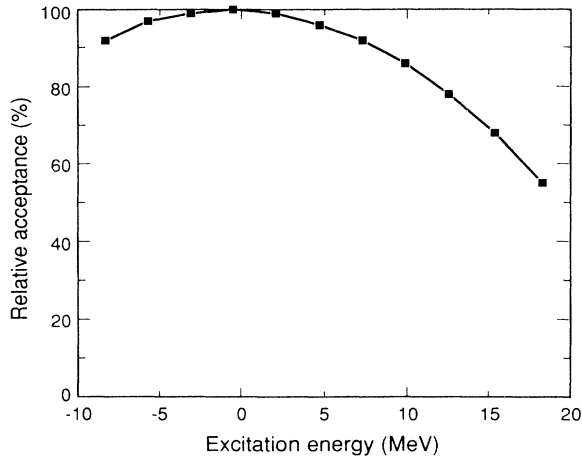


FIG. 2. Measured relative detector acceptance as a function of excitation energy, for  $\pi^+$  scattering at 180 MeV and  $60^\circ$ . The relative angular acceptance of the spectrometer is scaled to 100% = 9.92 msr and the excitation energy is determined from the focal-plane position via the momentum of the scattered pion.

along the focal plane was obtained from a measurement of  $\pi^+$  elastic scattering from carbon, and is shown in Fig. 2. The acceptance is a strong function of the position of the detected scattered pion along the focal plane of the spectrometer, and decreases precipitously as one approaches the edge of the focal plane. The inelastic data were analyzed in 2-MeV bins, and by comparing nominally identical runs, the data were found to be quite reliable up to 10 MeV above the two-body-breakup thresholds (6.3 MeV for  ${}^3\text{H}$  and 5.5 MeV for  ${}^3\text{He}$ ). (Above this excitation energy, the increasingly large background subtractions, together with the approach to the edge of the focal plane, resulted in fluctuations which were too large to allow one to extract reliable results.) Thus, the cross sections reported here are integrated over the energy bins from 6.3 to 16.3 MeV for  ${}^3\text{H}$  and from 5.5 to 15.5 MeV for  ${}^3\text{He}$ . The breakup energies for  ${}^3\text{H}$  (6.3 MeV) and  ${}^3\text{He}$  (5.5 MeV) are not the same because of the  $n$ - $p$  mass difference and the difference in Coulomb

energy. The differences in Coulomb energy between the  $n$ - $d$  or  $n$ - $n$ - $p$  final states for  ${}^3\text{H}$  (only one charged particle in the final states) and the  $p$ - $d$  or  $p$ - $p$ - $n$  final states for  ${}^3\text{He}$  (two charged particles in the final states) also should be taken into account. Fortunately, the effect of the different breakup energies largely compensates for that of the different Coulomb energies.

### III. RESULTS

#### A. Cross-section ratios

The ratios of cross sections which require only the relative monitoring of the incident beam and correction for differences in acceptance (see Fig. 2) are

$$\rho_+ = d\sigma(\pi^+ - {}^3\text{H})/d\sigma(\pi^+ - {}^3\text{He})$$

and

$$\rho_- = d\sigma(\pi^- - {}^3\text{H})/d\sigma(\pi^- - {}^3\text{He}) .$$

These ratios have much smaller systematic uncertainties (of the order of a few tenths of a percent, essentially arising only from the uncertainties in the sample masses) than do the simple charge-symmetric ratios  $r_1$  and  $r_2$  (for which the systematic uncertainties are of the order of a few percent, arising from the difference in monitoring of the  $\pi^+$  and the  $\pi^-$  beams).

The superratio  $R = r_1 r_2 = \rho_+ \rho_-$  is likewise independent of relative pion-beam monitoring, but involves all four cross sections (instead of just two of them), which therefore approximately doubles the statistical uncertainties arising from background subtractions. The observed large deviation of  $R$  from unity for elastic scattering (Refs. [1-5]) is evidence for the violation of charge symmetry. The results for the ratios of the inelastic-scattering cross sections are given in Table I.

The quantity  $\rho_+$  is the one measured with both the best relative precision and the best absolute accuracy, because the  $\pi^+$  beam is about five times as intense as the  $\pi^-$  beam and the  ${}^3\text{H}$  target contains twice as many atoms as the  ${}^3\text{He}$  target. Thus, we compare, in Fig. 3, the values for  $\rho_+$  (or the weighted average of  $\rho_+$  and  $1/\rho_-$ ) determined from the inelastic data of the present experiment (and a previously unpublished point at 180 MeV by

TABLE I.  $\pi^\pm$  trinucleon inelastic cross-section ratios.

	$r_1$	$r_2$	$\rho_+$	$\rho_-$	$P_t$	$P_r$	$R$
$T_\pi = 142$ MeV							
$\theta_{\text{lab}} = 40^\circ$	0.97(29)	1.03(18)	0.42(9)	2.37(57)	2.45(49)	2.30(65)	1.00(31)
$60^\circ$	0.99(16)	0.96(7)	0.47(4)	2.02(23)	2.04(16)	2.10(32)	0.95(15)
$80^\circ$	0.81(12)	1.29(12)	0.53(4)	1.95(25)	2.42(23)	1.52(23)	1.03(16)
$90^\circ$	1.06(24)	1.08(15)	0.56(7)	2.03(39)	1.90(25)	1.89(41)	1.14(26)
$110^\circ$	0.85(24)	1.07(13)	0.54(5)	1.68(44)	1.97(24)	1.56(44)	0.91(26)
$T_\pi = 180$ MeV							
$\theta_{\text{lab}} = 40^\circ$	0.94(11)	0.95(8)	0.51(4)	1.74(18)	1.85(14)	1.83(22)	0.89(12)
$60^\circ$	0.76(8)	1.07(9)	0.58(4)	1.38(15)	1.83(17)	1.30(14)	0.81(10)
$80^\circ$	1.19(19)	0.99(10)	0.73(6)	1.60(22)	1.35(12)	1.62(26)	1.18(19)
$110^\circ$	1.14(35)	0.87(17)	0.74(11)	1.33(37)	1.17(20)	1.53(49)	0.99(31)
$T_\pi = 220$ MeV							
$\theta_{\text{lab}} = 40^\circ$		0.79(6)	0.38(3)		2.05(17)		
$60^\circ$	1.12(23)	1.02(9)	0.72(6)	1.59(27)	1.42(13)	1.56(30)	1.14(23)
$80^\circ$	1.41(56)	1.05(31)	0.90(21)	1.64(57)	1.17(25)	1.56(65)	1.48(59)

the authors of Ref. [3]) with the values for  $\rho_+$  determined from the elastic data of Refs. [3–5]. It is readily apparent that the inelastic data remain nearly constant while the elastic data vary substantially. The values for  $\rho_-$  for the inelastic data also remain constant, with greater experimental uncertainties (mostly statistical), while those for the elastic data again vary substantially.

The quantities  $\rho_+$  and  $\rho_-$  are ratios of cross sections that have been shifted in energy, because of the different breakup energies for  $^3\text{H}$  and  $^3\text{He}$ . This procedure introduces an additional uncertainty of several percent. There is no energy shift, however, for the ratios

$$P_t = d\sigma(\pi^- - ^3\text{H})/d\sigma(\pi^+ - ^3\text{H})$$

and

$$P_r = d\sigma(\pi^+ - ^3\text{He})/d\sigma(\pi^- - ^3\text{He}).$$

In fact, these ratios also are structureless for inelastic scattering, and their ratio  $P_t/P_r$  agrees with  $\rho_+/\rho_-$ , showing that the use of  $\rho_+/\rho_-$  does not produce misleading results because of the energy shift. (Specifically, within experimental uncertainties,  $P_t/P_r$  agrees with  $\rho_+/\rho_-$  for 8 of the 12 measured points, is slightly

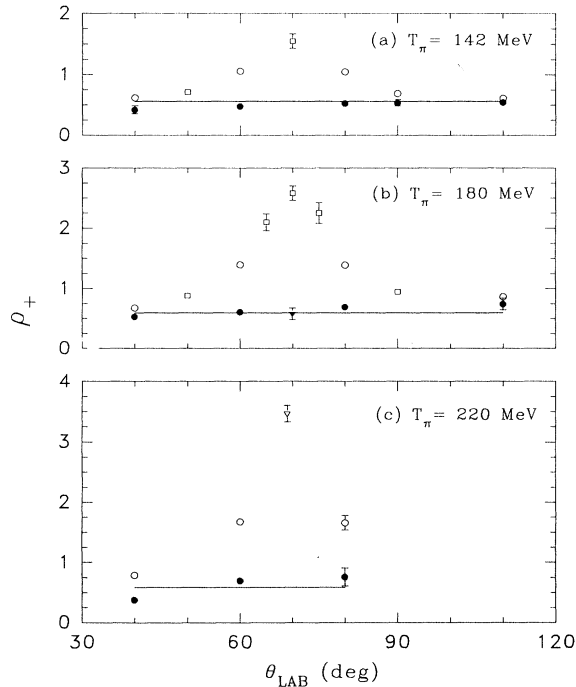


FIG. 3. The ratio  $\rho_+$  (see text) for (a)  $T_\pi = 142$  MeV; (b) for 180 MeV; and (c) for 220 MeV. The open symbols represent the elastic-scattering data from Ref. [3] (squares), Ref. [4] (circles), and Ref. [5] (triangle); the solid symbols represent the inelastic-scattering data from the present measurement (circles), and an unpublished datum from Ref. [3] (triangle). The present data (solid circles) represent the weighted average of  $\rho_+$  and  $1/\rho_-$  in order to minimize both statistical and systematic uncertainties; in nearly all cases, these averages are indistinguishable from the values of  $\rho_+$  alone. The solid lines connect points calculated from  $\pi$ -N data [6] assuming no nuclear-medium effects.

larger for 3, and slightly smaller for 1.)

The simple ratios  $r_1$  and  $r_2$  and the superratio  $R$  for the inelastic-scattering data reported here are typically consistent with unity, while the values for  $r_2$  and  $R$  for the elastic-scattering data in this angular range almost all lie two or more standard deviations above unity [4].

## B. Cross sections

The measured doubly differential cross sections [in  $\text{mb}/(\text{sr } 10 \text{ MeV})$ ] for the inelastic scattering of charged pions from  $^3\text{H}$  and  $^3\text{He}$  are listed in Table II and shown in Figs. 4–6: Fig. 4(a) shows the cross sections for  $\pi^+ - ^3\text{H}$  and  $\pi^- - ^3\text{He}$  for  $T_\pi = 142$  MeV as a function of center-of-mass angle  $\theta_{\text{c.m.}}$ ; Fig. 4(b) shows the cross sections for  $\pi^- - ^3\text{H}$  and  $\pi^+ - ^3\text{He}$ , with a scale change of a factor of 2 for comparison purposes; Figs. 5(a) and (b) show the same cross sections, but for  $T_\pi = 180$  MeV; and Figs. 6(a) and (b) show the cross sections for 220 MeV.

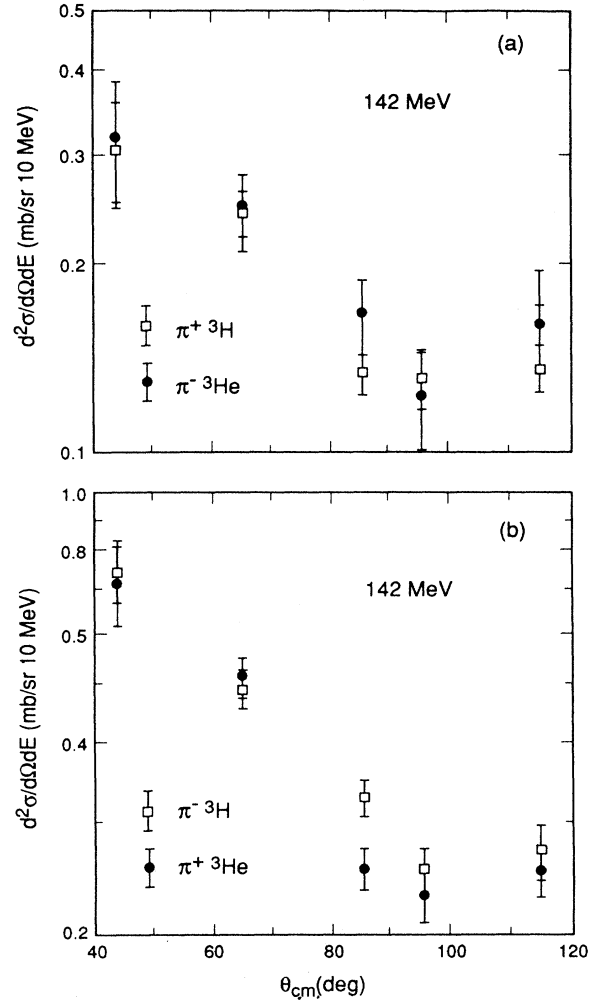
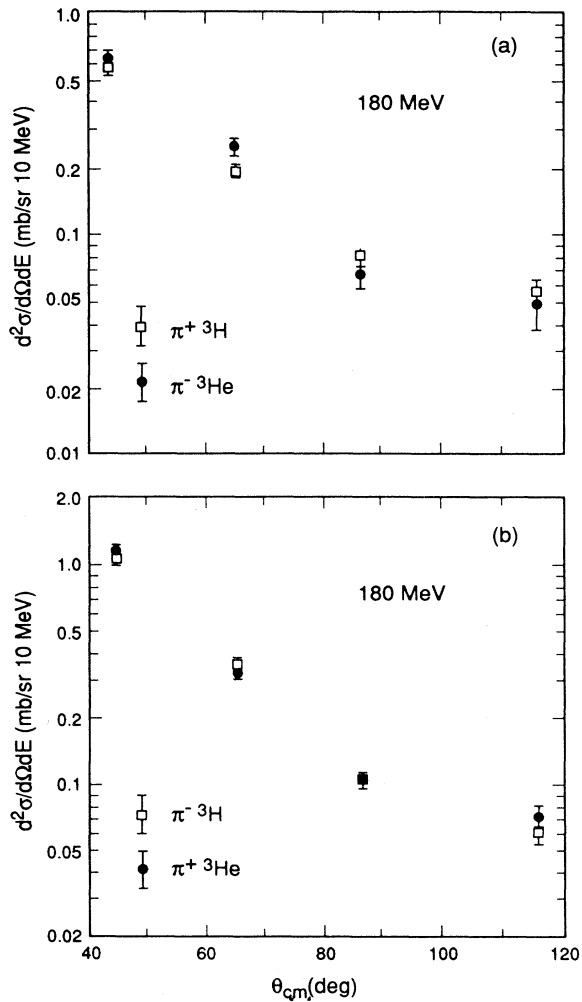
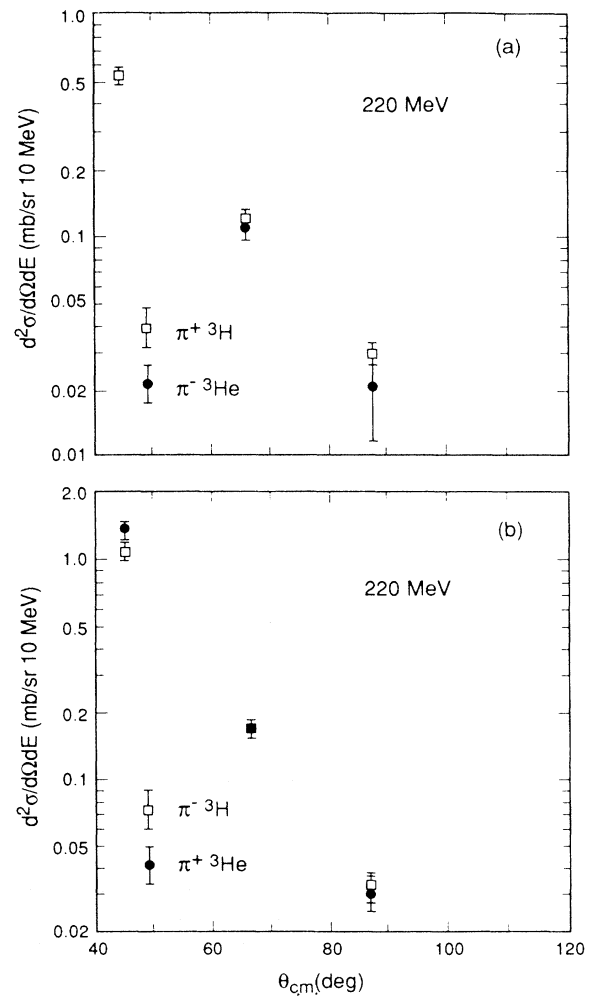


FIG. 4. (a) The integrated-over-energy (see text) doubly differential cross sections for inelastic  $\pi^+ - ^3\text{H}$  and  $\pi^- - ^3\text{He}$  scattering as a function of center-of-mass scattering angle for  $T_\pi = 142$  MeV; (b) for  $\pi^- - ^3\text{H}$  and  $\pi^+ - ^3\text{He}$ . The 10-MeV energy interval runs from 6.3 to 16.3 MeV for  $^3\text{H}$  and from 5.5 to 15.5 MeV for  $^3\text{He}$ .

TABLE II.  $\pi^\pm$  trinucleon inelastic cross sections [mb/(sr 10 MeV)].

		$\pi^+ - ^3\text{H}$	$\pi^- - ^3\text{He}$	$\pi^- - ^3\text{H}$	$\pi^+ - ^3\text{He}$
$T_\pi = 142$ MeV					
$\theta_{\text{lab}} =$	40°	0.305(54)	0.316(71)	0.747(71)	0.728(109)
	60°	0.242(20)	0.244(34)	0.493(35)	0.513(39)
	80°	0.135(11)	0.168(23)	0.328(22)	0.255(18)
	90°	0.132(14)	0.124(23)	0.252(22)	0.234(24)
	110°	0.137(12)	0.161(35)	0.271(26)	0.252(22)
$T_\pi = 180$ MeV					
$\theta_{\text{lab}} =$	40°	0.589(46)	0.628(69)	1.090(74)	1.151(92)
	60°	0.192(13)	0.254(22)	0.352(21)	0.329(21)
	80°	0.078(6)	0.066(9)	0.105(8)	0.107(9)
	110°	0.053(6)	0.047(12)	0.062(7)	0.072(11)
$T_\pi = 220$ MeV					
$\theta_{\text{lab}} =$	40°	0.538(46)		1.102(77)	1.402(99)
	60°	0.124(10)	0.111(17)	0.176(14)	0.173(15)
	80°	0.029(3)	0.021(9)	0.034(6)	0.032(6)

FIG. 5. (a) and (b) same as Fig. 4, but for  $T_\pi = 180$  MeV.FIG. 6. (a) and (b) same as Fig. 4, but for  $T_\pi = 220$  MeV.

One can make several observations from these data. First, a cursory comparison of the pair of cross sections shown in each of the six plots shows that they are substantially the same, and indeed, this would be expected if the cross sections were nearly charge symmetric, in the absence of large asymmetric Coulomb effects. Second, a rough comparison of the (a) plots with the (b) plots shows that the cross sections shown in the latter plots are approximately twice as large as those shown in the former; this would be expected if the pion-trinucleon cross sections were dominated by the elementary pion-nucleon amplitudes at or near the  $\Delta$  resonance, since there are twice as many neutrons and half as many protons in  ${}^3\text{H}$  as there are in  ${}^3\text{He}$ , and if the  $\pi^+-n$  and  $\pi^-p$  amplitudes were unimportant and could be neglected. Third, a more careful comparison of the (a) plots with the (b) plots reveals that the cross sections in the latter are not quite twice as large as those in the former, but fall about 15% short of that value; this would be expected if the  $\pi^+-n$  and  $\pi^-p$  amplitudes were about one-third as large as those for  $\pi^+p$  and  $\pi^-n$ , which in fact they are.

To be more quantitative, the cross-section ratios  $\rho_+$  (or  $1/\rho_-$ ) were calculated from tabulated  $\pi^+p$  and  $\pi^-p$  data (Ref. [6]), assuming that  $d\sigma(\pi^+-n) = d\sigma(\pi^-p)$  and  $d\sigma(\pi^-n) = d\sigma(\pi^+p)$  and that no nuclear-medium effects play a role. The calculated results are shown as the solid lines in Fig. 3, and are nearly independent of angle for a given pion energy:  $0.60 \pm 0.02$  for 142 MeV and  $0.58 \pm 0.01$  for 180 and for 220 MeV. The average experimental values for  $\rho_+$  and  $1/\rho_-$  are  $0.51 \pm 0.06$  for 142 MeV,  $0.65 \pm 0.08$  for 180 MeV, and  $0.61 \pm 0.15$  for 220 MeV. Even this rudimentary calculation agrees remarkably well with the data.

Finally, perhaps in all cases but certainly in most, the  ${}^3\text{H}$  cross sections fall off somewhat more slowly with angle, and hence with increasing momentum transfer, than do those for  ${}^3\text{He}$ . This would be expected if the size of  ${}^3\text{H}$  were smaller than that of  ${}^3\text{He}$ , which in fact it is. Gibbs and Gibson [7] have analyzed the superratio data of Refs. [3,4] to find that the source of the charge asymmetry is just this—that the neutron radius of  ${}^3\text{H}$  is  $0.030 \pm 0.010$  fm smaller than the proton radius of  ${}^3\text{He}$  and the proton radius of  ${}^3\text{H}$  is  $0.035 \pm 0.007$  fm smaller than the neutron radius of  ${}^3\text{He}$ .

#### IV. DISCUSSION

##### A. Comparison with elastic pion scattering

Inelastic pion scattering at low to medium energies can be characterized in two ways, depending on whether the process is dominated by pion scattering from the nucleus as a whole (incoherent but quasibound) or from the individual nucleons in the nucleus (quasifree). The former case holds for barely inelastic scattering, where the recoil involves all or most of the nucleons in the nucleus, and the latter for quasifree scattering, where the recoiling body is a single nucleon.

It is illustrative to compare the kinematics of the scattered pion for  $\pi^-{}^3\text{H}$  and  $\pi^-p$  elastic scattering, as can be seen in Table III. Quasifree scattering resembles the kinematics

TABLE III. Kinetic energy (in MeV) of the scattered pion for  $T_\pi = 180$  MeV.

$\theta_{\text{lab}}$	$\pi^-{}^3\text{H}$	$\pi^-p$
$40^\circ$	172	161
$60^\circ$	166	141
$80^\circ$	155	124
$110^\circ$	146	98

of free  $\pi^-p$  scattering, with a small energy shift that depends on the assumed Fermi momentum distribution. For  $\pi^-{}^3\text{H}$ , this is about 6 MeV, which is accounted for by the binding energy [8,9]. The values in Table III show that with the possible exception of  $\theta_{\text{lab}} = 40^\circ$ , this experiment is concerned with barely inelastic scattering, since we report on pion results that are only 6–16 MeV from elastic scattering.

(1) For barely inelastic scattering, the kinematics of the scattered pion are very similar to those for elastic scattering except that the kinetic energy is some 10 MeV or so less; this requires that the recoil nucleus break up but that the fragments have very little relative momentum. The data presented here belong in this category. In the impulse approximation, the cross section for barely inelastic scattering is the incoherent sum of  $\pi^-p$  and  $\pi^-n$  scattering times the probability for finding the nucleus in the appropriate kinematic state, for which we will use the appropriate nuclear form factors. For  $\pi^+{}^3\text{H}$  scattering, for example, the lowest-order approximation is

$$d\sigma[\pi^+{}^3\text{H}]^* \cong \Gamma^* [d\sigma(\pi^+p \rightarrow \pi^+p)|F_p|^2 + 2d\sigma(\pi^+n \rightarrow \pi^+n)|F_n|^2], \quad (1)$$

where the asterisk indicates that we are considering barely inelastic scattering.  $\Gamma^*$  is a correction factor for three-body kinematics, nuclear shadowing, and final-state interactions;  $F_p$  is the proton matter form factor for  ${}^3\text{H}$  and  $F_n$  is its neutron matter form factor. With this approximation, we obtain for the ratio of barely inelastic-scattering cross sections

$$P_t^* = \frac{2d\sigma(\pi^-n)|F_n|^2 + d\sigma(\pi^-p)|F_p|^2}{2d\sigma(\pi^+n)|F_n|^2 + d\sigma(\pi^+p)|F_p|^2} \quad (2)$$

in which the strong final-state interactions partly cancel one another (although the electromagnetic ones do not). This ratio also is less subject to experimental uncertainties than is the absolute cross section.

In the region of the  $\Delta(1232)$  resonance, we have the following approximate relation:

$$d\sigma(\pi^+n) \cong \frac{1}{9}d\sigma(\pi^+p).$$

If we make the simplifying assumption that

$$F_p^2 = [1 - \varepsilon(t)]F_n^2, \quad (3)$$

we obtain the ratio

$$P_t^* \cong 1.7[1 + 0.8\varepsilon(t)]. \quad (4)$$

Our experimental results for  $P_t$  are given in Table I. They

show that at each energy  $\varepsilon$  varies monotonically with  $t$ , which implies that the proton form factor for  ${}^3\text{H}$  differs from the neutron form factor, and that the difference depends smoothly on  $t$ . This is consistent with the detailed calculation of Ref. [7].

(2) For quasifree scattering, the pion interacts primarily with one quasifree nucleon. The energy loss of the pion is comparable to that for scattering on a free nucleon, and is much more than it is for barely inelastic scattering. The cross section is the incoherent sum of the free pion-nucleon elastic-scattering cross sections, modified by nuclear-medium effects, including the Fermi momentum of the initial-state nucleon, a reduced effective nucleon mass to account for nuclear binding, and multiple scattering. The cross section depends only weakly and rather indirectly on the nuclear wave function. Thus, in the lowest-order approximation,

$$d\sigma[\pi^+{}^3\text{H}]^{**} \cong \Gamma^{**}[2d\sigma(\pi^+n) + d\sigma(\pi^+p)] \quad (5)$$

evaluated at the appropriate energy, the double asterisk indicating a quasifree-scattering process. From Eq. (5) we obtain the ratio of cross sections

$$P_t^{**} = \frac{2d\sigma(\pi^-n) + d\sigma(\pi^-p)}{2d\sigma(\pi^+n) + d\sigma(\pi^+p)}. \quad (6)$$

Experimental data for the ratio  $P_t^{**}$  for the related case of pion quasifree scattering on  ${}^3\text{He}$  in this energy region has been obtained at PSI and LAMPF [8,9]. The chief difference between  $P_t^*$  and  $P_t^{**}$  (or between  $P_\tau^*$  and  $P_\tau^{**}$ ) is the angular dependence, which reflects the fact that barely inelastic scattering depends critically on the nuclear wave function. In our approach, this dependence is expressed via the ratio of the matter form factors. On the other hand, quasifree scattering is insensitive to the nuclear wave function, and the ratio  $P_\tau^{**}$  agrees very well with the ratio of the elementary  $\pi$ - $N$  cross sections (see Ref. [9]). Comparison of Eqs. (1) and (5) shows that the cross section for barely inelastic scattering is expected to be much smaller than that for quasifree scattering. This is in accord with measurement.

Here we wish to compare barely inelastic with elastic pion scattering. The cross section for the latter depends on the coherent sum of the elementary  $\pi$ - $N$  non-spin-flip and spin-flip amplitudes  $f$  and  $g$ , respectively, and also must reflect the effects of Pauli blocking resulting from the antiparallel orientation of the spins of the paired nucleons, e.g., the two neutrons in  ${}^3\text{H}$ . In the impulse approximation, as discussed in Ref. [3],

$$\begin{aligned} d\sigma(\pi^+{}^3\text{H} \rightarrow \pi^+{}^3\text{H}) \cong \Gamma\{ & |f(\pi^+p)F_p({}^3\text{H}) \\ & + 2f(\pi^+n)F_n({}^3\text{H})|^2 \\ & + |g(\pi^+p)F_p({}^3\text{H})|^2 \}. \end{aligned} \quad (7)$$

As noted above, the angular dependence of the non-spin-flip and spin-flip amplitudes,  $f \sim 2 \cos \theta$  and  $g \sim \sin \theta$ , results in the non-spin-flip dip in  $P_t$  at  $\theta = 90^\circ$  in the  $\pi$ - $N$  system, which is at about  $78^\circ$  in the  $\pi$ - ${}^3\text{H}$  system. Following Ref. [3], we have

$$\begin{aligned} P_t &= \frac{d\sigma(\pi^-{}^3\text{H} \rightarrow \pi^-{}^3\text{H})}{d\sigma(\pi^+{}^3\text{H} \rightarrow \pi^+{}^3\text{H})} \\ &\cong 0.9 \frac{(\frac{1}{3} + 2\alpha_t)^2 + \frac{1}{9} \cdot \frac{1}{4} \tan^2 \theta}{(1 + \frac{2}{3}\alpha_t)^2 + \frac{1}{4} \tan^2 \theta}, \end{aligned} \quad (8)$$

where 0.9 is the ratio of nuclear shadowing corrections,  $g/f \cong \frac{1}{2} \tan \theta$ , and  $\alpha_t = F_n/F_p$ . The experimental values for the weighted average of  $P_t$  and  $P_\tau$  from Refs. [3-5] are shown in Fig. 7, together with the evaluation of Eq. (8), and are compared with the present data for the weighted average of  $P_t^*$  and  $P_\tau^*$ . The spectacularly different angular dependence of the ratios  $P_t$  and  $P_t^*$  clearly illustrates the usefulness of the impulse-approximation calculation for ratios of cross sections.

The cross sections themselves for elastic (Fig. 6 in Ref. [4]) and inelastic (Figs. 4-6 above) scattering can be compared as well. The gross features at  $T_\pi = 180$  and 220 MeV are in reasonable correspondence, but at  $T_\pi = 142$  MeV there is a marked difference between elastic and barely inelastic pion scattering which is not understood at present.

## B. Comparison with inelastic electron scattering

Finally, it is of interest to compare our barely inelastic pion-scattering results to barely inelastic electron-

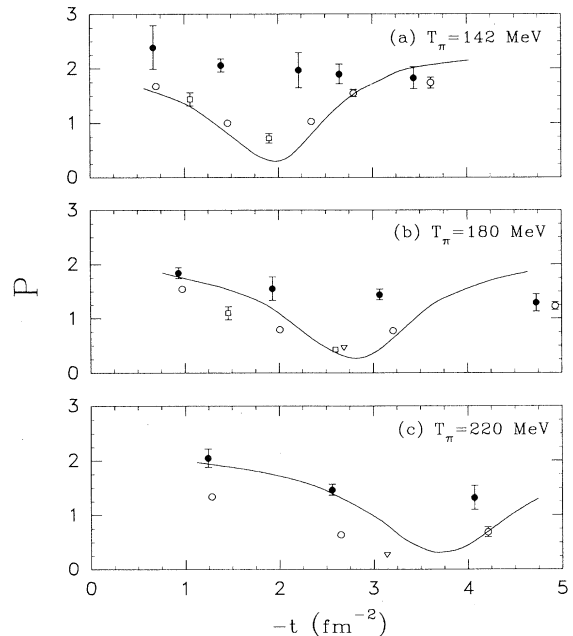


FIG. 7. Weighted average of the ratios  $P_t$  and  $P_\tau$  for the elastic-scattering data of Refs. [3-5] (open symbols, as in Fig. 3) and  $P_t^*$  and  $P_\tau^*$  for the present inelastic-scattering data (solid circles). The curves are evaluations of Eq. (8) (for elastic scattering), which, strictly speaking, are valid only for 180 MeV. (a) show the data for  $T_\pi = 142$  MeV, (b) for 180 MeV, and (c) for 220 MeV.

scattering data which have become available with the work of Retzlaff *et al.* [10]. The data are given in Tables IV and V as functions of both the four-momentum transfer  $-t$  and the total center-of-mass energy  $\sqrt{s}$ . Figure 8 shows our pion double-differential cross-section data and

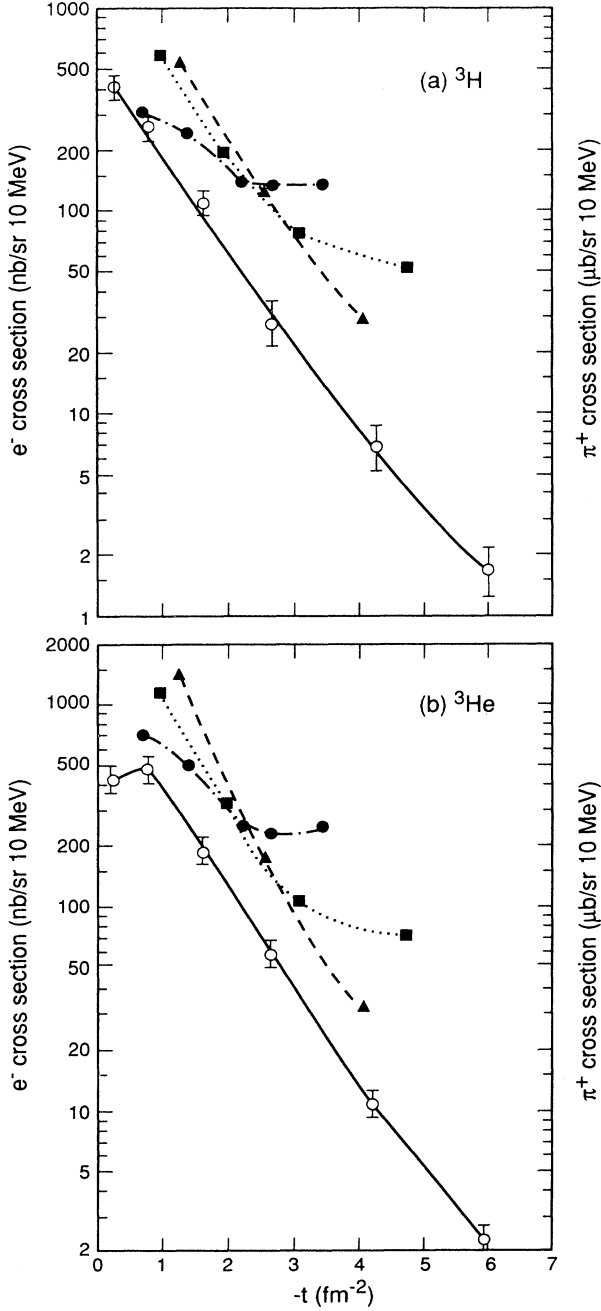


FIG. 8. (a) Cross sections for  $e^-$  scattering from  ${}^3\text{H}$  (open symbols, from Ref. [10]), compared with those for  $\pi^+$  scattering at  $\sqrt{s} = 3.081$  GeV (solid circles), 3.115 GeV (solid squares), and 3.151 GeV (solid triangles), vs  $-t$ ; (b) the same for  ${}^3\text{He}$ . The lines merely guide the eye.

TABLE IV. Cross sections (for error bars see Table II) vs  $-t$  and  $\sqrt{s}$  [ $\text{mb}/(\text{sr } 10 \text{ MeV})$ ].

$-t$ ( $\text{fm}^{-2}$ )	$\sqrt{s}$ (GeV)	$\pi^+ - {}^3\text{H}$	$\pi^- - {}^3\text{He}$	$\pi^- - {}^3\text{H}$	$\pi^+ - {}^3\text{He}$
0.67	3.081	0.305	0.316	0.747	0.728
0.93	3.115	0.589	0.628	1.090	1.151
1.24	3.151	0.538		1.102	1.402
1.39	3.081	0.242	0.244	0.493	0.513
1.93	3.115	0.192	0.254	0.352	0.329
2.22	3.081	0.135	0.168	0.328	0.255
2.56	3.151	0.124	0.111	0.176	0.173
2.65	3.081	0.132	0.124	0.252	0.234
3.07	3.115	0.078	0.066	0.105	0.107
3.44	3.081	0.137	0.161	0.271	0.252
4.07	3.151	0.029	0.021	0.034	0.032
4.73	3.115	0.053	0.047	0.062	0.072

the electron-scattering data obtained at  $\theta_L = 54^\circ$  at different incident energies, plotted as a function of the four-momentum transfer. In the impulse approximation we have

$$d\sigma[e^- - {}^3\text{H}]^* \cong \Gamma^* \sigma_M |F_c|^2,$$

where  $\sigma_M$  is the Mott cross section and  $F_c$  is the charge form factor. Since  $F_c$  and  $F_p$  should have nearly the same  $t$  dependence, we anticipate that the barely inelastic cross sections for pions and electrons will have a similar  $t$  dependence in the appropriate kinematic region. This appears to be the case at  $T_\pi = 220$  MeV but not so at  $T_\pi = 180$  MeV in the backward direction. At  $T_\pi = 142$  MeV, the cross-section shapes are totally different. Perhaps this should not be surprising, since the elastic and barely inelastic cross sections are different as well. One factor that probably contributes to the lack of correspondence in shape is that the pion data should exhibit interference between  $s$ - and  $p$ -wave scattering while the electron data do not. (Diffraction minima for both would occur only at a much larger momentum transfer.) A full analysis of the comparison between barely elastic electron and pion scattering will be the subject of a separate work.

TABLE V. Electron-scattering cross sections vs  $-t$  and  $\sqrt{s}$  [ $\text{nb}/(\text{sr } 10 \text{ MeV})$ ].

$-t$ ( $\text{fm}^{-2}$ )	$\sqrt{s}$ (GeV)	$e^- - {}^3\text{H}$	$e^- - {}^3\text{He}$
0.23	2.92	413(34)	434(36)
0.77	3.00	266(24)	492(37)
1.62	3.08	109(11)	188(17)
2.64	3.16	27.3(48)	58.3(69)
4.27	3.24	6.9(16)	10.9(19)
5.98	3.32	1.7(5)	2.3(6)
8.10	3.40	0.4(2)	0.4(2)
11.70	3.51	0.05(7)	0.06(10)

## ACKNOWLEDGMENTS

We thank J. Van Dyke, H. R. Maltrud, and L. L. Sturgess for their expert technical help and S. Graessle and K. Mitchell for their help in taking the data.

This work was supported in part by the U.S. Department of Energy and the National Science Foundation under Grants DE-FG05-86ER40285 and NSF-PHY-8604524 and Contracts DE-AS03-81ER40021 and DE-AS05-81ER40036.

- 
- [1] B. M. K. Nefkens, W. J. Briscoe, A. D. Eichon, D. H. Fitzgerald, J. A. Hall, A. Mokhtari, and J. A. Wightman, *Phys. Rev. Lett.* **52**, 735 (1984).
  - [2] C. Pillai, D. B. Barlow, B. L. Berman, W. J. Briscoe, A. Mokhtari, B. M. K. Nefkens, A. M. Petrov, and M. E. Sadler, *Phys. Lett. B* **207**, 389 (1988).
  - [3] B. M. K. Nefkens, W. J. Briscoe, A. D. Eichon, D. H. Fitzgerald, A. Mokhtari, J. A. Wightman, and M. E. Sadler, *Phys. Rev. C* **41**, 2770 (1990).
  - [4] C. Pillai, D. B. Barlow, B. L. Berman, W. J. Briscoe, A. Mokhtari, B. M. K. Nefkens, and M. E. Sadler, *Phys. Rev. C* **43**, 1838 (1991).
  - [5] K. S. Dhuga *et al.*, *Phys. Rev. C* (to be submitted).
  - [6] Program SAID at the LAMPF Data Analysis Center, from R. Arndt, VPI  $\pi$ -N data PN892, June 1989.
  - [7] W. R. Gibbs and B. F. Gibson, *Phys. Rev. C* **43**, 1012 (1991).
  - [8] A. Klein, C. Gysin, R. Henneck, J. Jourdan, M. Pickar, G. R. Plattner, I. Sick, and J. P. Egger, *Nucl. Phys.* **A472**, 605 (1987).
  - [9] R. R. Whitney, J. Källne, J. S. McCarthy, R. C. Minehart, R. L. Boudrie, J. F. Davis, J. B. McClelland, and S. Stetz, *Nucl. Phys.* **A408**, 417 (1983).
  - [10] G. A. Retzlaff, H. S. Caplan, E. L. Hallin, D. M. Skopik, D. Beck, K. I. Blomqvist, G. Dobson, K. Dow, M. Farkhondeh, J. Flanz, S. Kowalski, W. W. Sapp, C. P. Sagent, D. Tieger, W. Turchinets, C. F. Williamson, W. Dodge, X. K. Maruyama, J. W. Lightbody, Jr., R. Goloskie, J. McCarthy, T. S. Ueng, R. R. Whitney, B. Quinn, S. Dytman, K. Von Reden, R. Schiavilla, and J. A. Tjon, *Phys. Rev. C* **49**, 1263 (1994), and G. A. Retzlaff, private communication.